Photocathode characterisation for robust PICOSEC Micromegas precise-timing detectors

M. Lisowska[a,b,*], R. Aleksan[c], Y. Angelis[d,e], S. Aune[c], J. Bortfeldt[f], F. Brunbauer[a], M. Brunoldi[g,h], E. Chatzianagnostou[d,e], J. Datta[i], K. Dehmelt[j], G. Fanourakis[k], S. Ferry[a], D. Fiorina[g,h,1], K. J. Floethner[a,l], M. Gallinaro[m], F. Garcia[n], I. Giomataris[c], K. Gnanvo[j], F.J. Iguaz[c,2], D. Janssens[a], A. Kallitsopoulou[c], M. Kovacic[o], B. Kross[j], C.C. Lai[p], P. Legou[c], J. Liu[q], M. Lupberger[l,r], I. Maniatis[a,d,3], J. McKisson[j], Y. Meng[q], H. Muller[a,r], R. De Oliveira[a], E. Oliveri[a], G. Orlandini[a,s], A. Pandey[j], T. Papaevangelou[c], M. Pomorski[t], M. Robert[a,u], L. Ropelewski[a], D. Sampsonidis[d,e], L. Scharenberg[a], T. Schneider[a], E. Scorsone[t], L. Sohl[a,c,4], M. van Stenis[a], Y. Tsipolitis[v], S. Tzamarias[d,e], A. Utrobicic[w], I. Vai[g,h], R. Veenhof[a], L. Viezzi[a], P. Vitulo[g,h], C. Volpato[a,x], X. Wang[q], S. White[y], W. Xi[j], Z. Zhang[q], Y. Zhou[q]

[a] *European Organization for Nuclear Research (CERN), 1211 Geneve 23, Switzerland,*
[b] *Université Paris-Saclay, F-91191 Gif-sur-Yvette, France,*
[c] *IRFU, CEA, Université Paris-Saclay, F-91191 Gif-sur-Yvette, France,*
[d] *Department of Physics, Aristotle University of Thessaloniki, University Campus, GR-54124, Thessaloniki, Greece,*
[e] *Center for Interdisciplinary Research and Innovation (CIRI-AUTH), Thessaloniki 57001, Greece,*
[f] *Department for Medical Physics, Ludwig Maximilian University of Munich, Am Coulombwall 1, 85748 Garching, Germany,*
[g] *Dipartimento di Fisica, Università di Pavia, Via Bassi 6, 27100 Pavia, Italy,*
[h] *INFN Sezione di Pavia, Via Bassi 6, 27100 Pavia, Italy,*
[i] *Department of Physics and Astronomy, Stony Brook University, Stony Brook, NY 11794-3800, USA,*
[j] *Jefferson Lab, 12000 Jefferson Avenue, Newport News, VA 23606, USA,*
[k] *Institute of Nuclear and Particle Physics, NCSR Demokritos, GR-15341 Agia Paraskevi, Attiki, Greece,*
[l] *Helmholtz-Institut für Strahlen- und Kernphysik, University of Bonn, Nußallee 14–16, 53115 Bonn, Germany,*
[m] *Laboratório de Instrumentacão e Física Experimental de Partículas, Lisbon, Portugal,*
[n] *Helsinki Institute of Physics, University of Helsinki, FI-00014 Helsinki, Finland,*
[o] *University of Zagreb, Faculty of Electrical Engineering and Computing, 10000 Zagreb, Croatia,*
[p] *European Spallation Source (ESS), Partikelgatan 2, 224 84 Lund, Sweden,*
[q] *State Key Laboratory of Particle Detection and Electronics, University of Science and Technology of China, Hefei 230026, China,*
[r] *Physikalisches Institut, University of Bonn, Nußallee 12, 53115 Bonn, Germany,*
[s] *Friedrich-Alexander-Universität Erlangen-Nürnberg, Schloßplatz 4, 91054 Erlangen, Germany,*
[t] *CEA-LIST, Diamond Sensors Laboratory, CEA Saclay, F-91191 Gif-sur-Yvette, France,*
[u] *Queen's University, Kingston, Ontario, Canada,*
[v] *National Technical University of Athens, Athens, Greece,*
[w] *Ruđer Bošković Institute, Bijenička cesta 54., 10 000 Zagreb, Croatia,*
[x] *Department of Physics and Astronomy, University of Florence, Via Giovanni Sansone 1, 50019 Sesto Fiorentino, Italy,*
[y] *University of Virginia, USA,*

Abstract

The PICOSEC Micromegas detector is a precise-timing gaseous detector based on a Cherenkov radiator coupled with a semi-transparent photocathode and a Micromegas amplifying structure, targeting a time resolution of tens of picoseconds for minimum ionising particles. Initial single-pad prototypes have demonstrated a time resolution below $\sigma = 25$ ps, prompting ongoing developments to adapt the concept for applications. The achieved performance is being transferred to robust multi-channel detector modules suitable for large-area detection systems requiring excellent timing precision. To enhance the robustness and stability of the PICOSEC Micromegas detector, research on robust carbon-based photocathodes, including Diamond-Like Carbon (DLC) and Boron Carbide (B_4C), is pursued. Results from prototypes equipped with DLC and B_4C photocathodes exhibited a time resolution of $\sigma \approx 32$ ps and $\sigma \approx 34.5$ ps, respectively. Efforts dedicated to improve detector robustness and stability enhance the feasibility of the PICOSEC Micromegas concept for large experiments, ensuring sustained performance while maintaining excellent timing precision.

Keywords: Gaseous detectors, Micromegas, Photocathodes, Timing resolution

1. Introduction

The intense interest in advancing technologies for precise-timing detectors has been driven by demanding environments

*Corresponding author.
Email address: marta.lisowska@cern.ch (M. Lisowska)

[1] Now at Gran Sasso Science Institute, Viale F. Crispi, 7 67100 L'Aquila, Italy.

[2] Now at SOLEIL Synchrotron, L'Orme des Merisiers, Départementale 128, 91190 Saint-Aubin, France.

[3] Now at Department of Particle Physics and Astronomy, Weizmann Institute of Science, Hrzl st. 234, Rehovot, 7610001, Israel.

[4] Now at TÜV NORD EnSys GmbH & Co. KG.

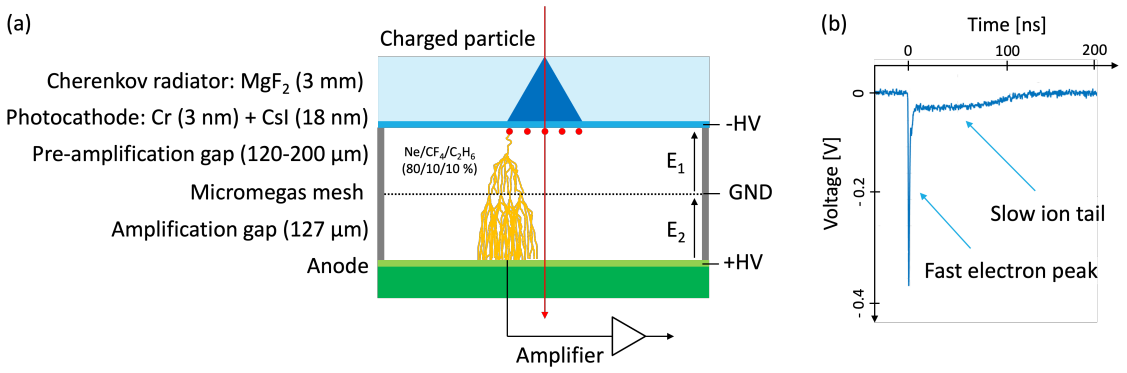

Figure 1: (a) PICOSEC detection concept: A charged particle passing through a Cherenkov radiator generates UV photons, which are converted into electrons on a photocathode. The electrons are multiplied in the gas volume in two stages and induce a signal on the anode. (b) Typical PICOSEC waveform: The signal displays a fast electron peak and a slow ion tail. Note that the figures are not drawn to scale [11].

anticipated in forthcoming High Energy Physics experiments. Meeting the criteria of achieving an excellent time resolution, ensuring stable long-term operation and providing large-area coverage is crucial for adapting the concept for physics applications. The PICOSEC Micromegas (hereafter PICOSEC) project [1] undertakes the efforts to develop a robust multi-channel gaseous detector, targeting a time resolution of $O(10)$ ps for Minimum Ionising Particles (MIPs). Initial single-pad prototypes equipped with a Cesium Iodide (CsI) photocathode have demonstrated a time resolution below $\sigma = 25$ ps [1], prompting further developments [2] - [13]. Although preliminary measurements of alternative approaches have been conducted previously [2, 5, 11, 13], a comprehensive characterisation of different carbon-based photocathodes has not been reported. This work aims to advance the development of robust photocathodes for PICOSEC detectors while maintaining an excellent time resolution.

Within the scope of this paper, measurements of three different photocathode materials, including CsI, Diamond-Like Carbon (DLC) and Boron Carbide (B_4C), are reported. The samples were manufactured by various research institutes, including the European Organization for Nuclear Research (CERN), the University of Science and Technology of China (USTC), the French Atomic Energy Commission (CEA) and the European Spallation Source (ESS).

2. PICOSEC Micromegas detection concept

The PICOSEC Micromegas detection concept is depicted in Fig. 1a [1]. The detector is designed to minimize time jitter from primary ionization in the gas by using a Cherenkov radiator. A charged particle passing through the crystal radiator generates a cone of ultraviolet (UV) photons which are partially converted into primary electrons on a photocathode coated on the window. Typically, the radiator in a PICOSEC detector is a 3 mm thick Magnesium Fluoride (MgF_2) crystal which transmits light above 120 nm. The window is coated with a 3 nm thick chromium (Cr) conductive interfacial layer that serves as a contact for the high voltage (HV). The UV photon-to-electron converter is an 18 nm thick semi-transparent CsI photocathode known for its high Quantum Efficiency (QE) for photons below 200 nm. All primary electrons are created at the same surface, eliminating uncertainty about the ionisation location and thereby minimising time jitter. The gas volume is filled with a mixture of 80% Ne, 10% CF_4 and 10% C_2H_6 at ambient pressure. The typical electric fields across the pre-amplification and amplification gaps are approximately 40 kV/cm and 20 kV/cm, correspondingly. In the presence of a strong electric field, the extracted electrons successively ionise gas molecules, causing electron multiplication, which first occurs in the pre-amplification gap and, after passing through the Micromegas mesh, continues in the amplification gap. The total gain achieved is on the level of $O(10^5 - 10^6)$. The amplified electrons move towards the anode, while the ions travel to the mesh. Their movement induce a signal on the anode, which is then amplified and read out by a digitiser. A typical PICOSEC waveform displaying a fast electron peak and a slow ion tail is illustrated in Fig. 1b. The leading edge of the electron peak determines a Signal Arrival Time (SAT).

Several optimisation studies were conducted on a 10 mm diameter active area single-pad PICOSEC detector to enhance high voltage stability, reduce noise, improve signal integrity and achieve uniform timing response, using a simplified assembly process [12]. The design includes improvements to the detector board, vessel, mechanical parts and electrical connections for both high voltage and signal. A new single-channel detector board is shown in Fig. 2.

To enhance the robustness and stability of the PICOSEC detector, research on robust photocathodes is underway. The initial prototype involved a CsI photocathode due to its high QE and UV sensitivity, nonetheless, the material is vulnerable to damage from ion blackflow, discharges and humidity. The robustness of the photocathode is crucial for maintaining detector efficiency and timing resolution during long-term operation. Potential alternatives include using protective layers or other materials, with carbon-based photocathodes like DLC and B_4C being the most promising candidates.

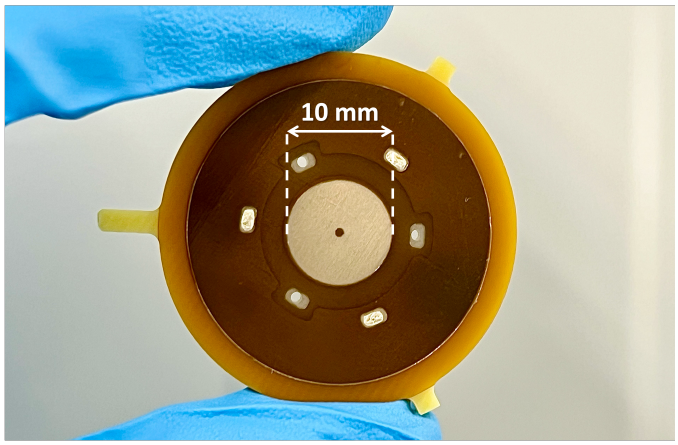

Figure 2: Single-channel detector board with a 10 mm diameter active area.

3. Experimental methodology

R&D activities within the PICOSEC project have covered aspects ranging from design and production, through assembly, to measurements in both laboratory conditions as well as with particle beams. Prototypes were assembled in a clean-room environment and tested in the laboratory. The ASSET (A Small Sample Evaporation Test) setup was developed to characterise photocathodes, facilitating transparency and QE measurements, as well as ageing studies [14, 15]. The time resolution of the detectors was evaluated using 150 GeV/c muon beams at the CERN SPS H4 beamline.

3.1. ASSET photocathode characterisation device

The ASSET setup was developed to characterise photocathodes for gaseous radiation detectors, as in the PICOSEC project [5]. The primary aims are to quantify QE and transparency of the photocathodes as well as their degradation due to ion backflow. Fig. 3 provides an overview of the ASSET setup.

Measurements utilise UV light from a system consisting of a deuterium lamp (McPherson, Model 632) and a Vacuum UltraViolet (VUV) monochromator (McPherson, Monarch). The system is flushed with high-purity nitrogen to prevent absorption of the short-wavelength portion of the UV spectrum. The monochromator is attached to the measurement chamber through an extension containing a collimating mirror chamber that focuses the light. A beam splitter divides the light into two beams. Two calibrated CsI photomultiplier tubes (PMTs) register the light intensity: one measures the amount of light at the sample position, while the other monitors light stability during measurements. The wavelength range for measurements is limited to about 140 nm on the low-wavelength side by the transparency of the MgF_2 lens and to about 200 nm on the high-wavelength side by the deuterium lamp's light intensity. The highest light intensity is observed at 160-180 nm.

The ASSET setup allows for measurements in reflective and transmission modes. In both modes, the extraction grids record the current generated by electrons extracted from the photocathodes. The reflective mode measures the QE of photocathodes, while the transmission mode evaluates both QE and transparency. The measurements are conducted in a vacuum of 10^{-6} mbar, achieved using pre-pumps and turbomolecular pumps. Additionally, the device enables the the collection of determined amounts of ion current on samples to study potential charge-induced ageing effects. Further details about the ASSET photocathode characterisation device can be found in [5].

The primary function of the ASSET setup is the measurement of photocurrent from photocathode samples. The QE is calculated from current measurements using the formula

$$QE = \frac{N_e}{N_{ph}} = \frac{\frac{I_s}{e}}{\frac{I_{PMT}}{e \cdot C_{PMT}}} = \frac{I_s \cdot C_{PMT}}{I_{PMT}}, \quad (1)$$

where N_e is the number of electrons extracted from the sample (measured on the sample), N_{ph} is the number of photons that arrive at the sample (measured with the PMT), I_s is the current measured on the sample (offset subtracted), I_{PMT} is the current measured on the PMT (offset subtracted), C_{PMT} is the calibration factor of PMT (depends on wavelength) and e is the elementary charge.

The current measured by the PMT is used to calculate the transparency (T) of the samples, given by

$$T = \frac{I_{PMT,\ s.\ in}}{I_{PMT,\ s.\ out}}, \quad (2)$$

where $I_{PMT,\ s.\ in}$ is the PMT current measured with the sample in the measurement position and $I_{PMT,\ s.\ out}$ is the PMT current measured with the sample out of measurement position. Transparency measurements in ASSET was performed in the VUV range between 140 nm and 200 nm. Transparency can also be assessed across the visible light spectrum, from 200 nm to 800 nm, using a spectrophotometer (PerkinElmer, Lambda 650 UV/VIS Spectrometer).

An important capability of the ASSET measurements is conducting ageing studies. The procedure starts with an X-ray beam entering the irradiation chamber filled with a gas mixture of Ar/CO_2 (70/30 %) at ambient pressure that ionises the gas and creates primary electrons. The primary electrons are attracted to multiplication wires, where an avalanche occurs in the high electric field region near the wires, producing additional electrons and ions. The electrons from he avalanche are collected on the wires, while the ions move towards the grounded sample. This process accumulates charge on the sample, allowing for the quantification of the drop in QE after exposure.

3.2. Characterisation with particle beams

Particle beam campaigns are conducted to measure the time resolution of prototypes assembled in various configurations. The measurements are conducted using 150 GeV/c muon beams at the CERN SPS H4 beamline. The test setup includes a beam telescope facilitating triggering, timing and tracking capabilities. An example telescope configuration is shown in Fig. 4. Precise particle tracking is achieved utilising three triple Gas Electron Multiplier (GEM) detectors with a spatial resolution below 80 µm. These devices use APV25

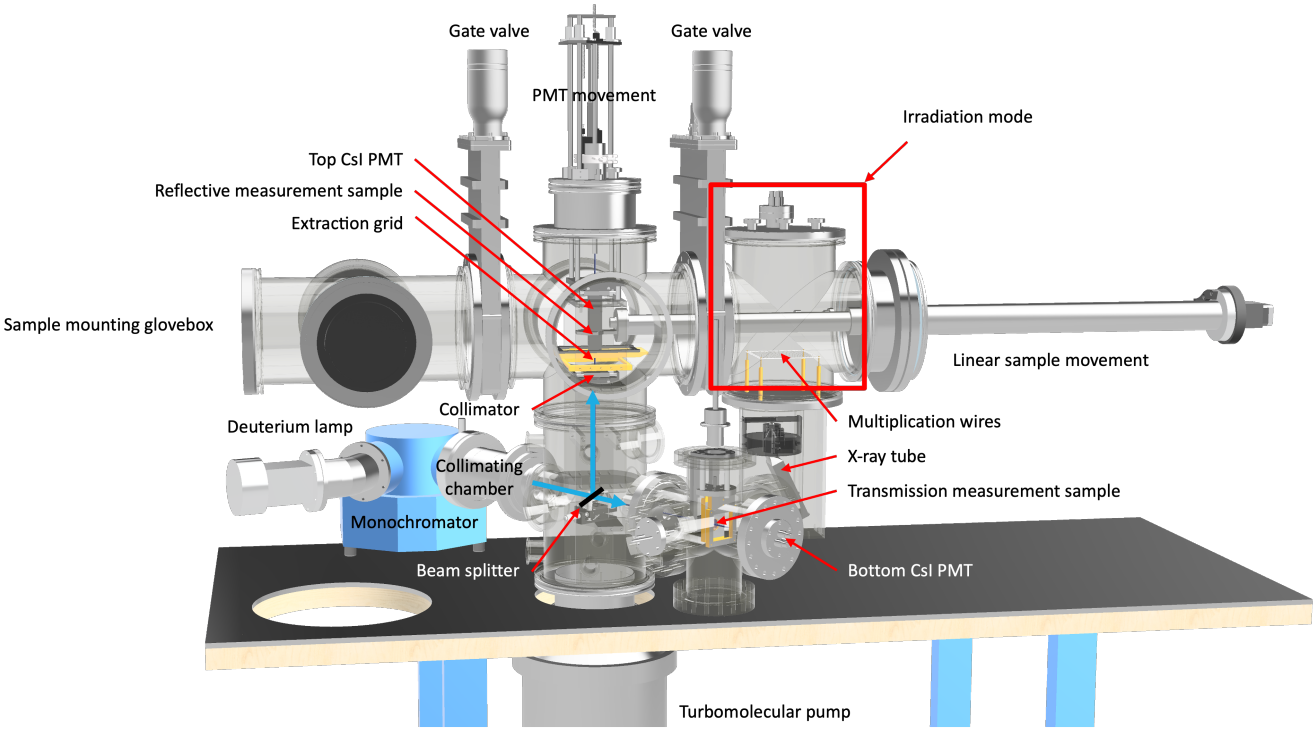

Figure 3: Overview of the ASSET photocathode characterisation device: The setup uses UV light from a deuterium lamp and a VUV monochromator, features a collimating mirror chamber, a beam splitter and two calibrated CsI PMTs to measure light intensity and stability within a wavelength range of 140-200 nm, peaking at 160-180 nm. It allows for measurements in reflective and transmission mode, as well as studies of the ageing process due to ion backflow [5].

front-end ASICs to shape the signals from all electrode channels, which are subsequently digitised using the Scalable Readout System (SRS) [16]. The GEMs are operated in a gas mixture of Ar/CO_2 (70/30 %) at ambient pressure. A micro-channel plate photomultiplier tube (MCP-PMT, Hamamatsu, R3809U-50) serves as the timing reference and data acquisition (DAQ) trigger. The telescope can be utilised for testing several PICOSEC prototypes simultaneously.

Different components individually contribute to the overall time resolution in a detector system, with the total time resolution being the sum of variances from each of these contributions. It can be represented by a simplified model

$$\sigma_{tot}{}^2 = \left(\frac{\sigma_{SPE}}{\sqrt{N_{PE}}}\right)^2 + \sigma_{t_0}{}^2 + \sigma_n{}^2 + ... \quad (3)$$

The first term is the time resolution of the PICOSEC prototype measured with MIPs, where σ_{SPE} is the time resolution achieved with SPE events and N_{PE} is the number of photoelectrons extracted from the photocathode [2]. The second term is the contribution of the reference device. The third term is the time jitter caused by noise in the detector and the connected external electrical circuit. The time resolutions discussed in this paper include contributions from all these components.

The photocathode performance is assessed by comparing N_{PE} they generate during the process. The number is estimated as the ratio of the signal amplitude induced by a single photoelectron (SPE) to the signal amplitude induced by a MIP. SPE measurements are performed using a light-emitting diode (LED), while the multiple photoelectron (MPE) measurements are conducted with muon beams. The signals are amplified by a custom-developed charge-sensitive ARTH amplifier [2] and read out by an oscilloscope (LeCroy WR8104, 10 GS/s sampling rate, 1 GHz bandwidth).

The procedure for calculating N_{PE} involves several steps. Firstly, the maximum amplitude for each waveform is determined. Secondly, a histogram of all maximum amplitudes is plotted. The noise component is fitted using a Gaussian distribution, while the signal component is fitted using an equation based on a Pólya distribution of the form

$$P_n = \frac{(\theta+1)^{\theta+1}}{\bar{n}\Gamma(\theta+1)}\left(\frac{n}{\bar{n}}\right)^{\theta} e^{-(\theta+1)n/\bar{n}}, \quad (4)$$

where: n is the number of charges produced, $\bar{n}$ the mean avalanche size, and θ the shape parameter. From this Pólya distribution, the mean value is calculated. Finally, the mean amplitude of the MPE is divided by the mean amplitude of the SPE to obtain the N_{PE} for a given photocathode. The N_{PE} is given by the formula

$$N_{PE} = \frac{V_{MIP}}{V_{SPE}}, \quad (5)$$

where V_{MIP} is a MIP mean amplitude, V_{SPE} is a SPE mean amplitude.

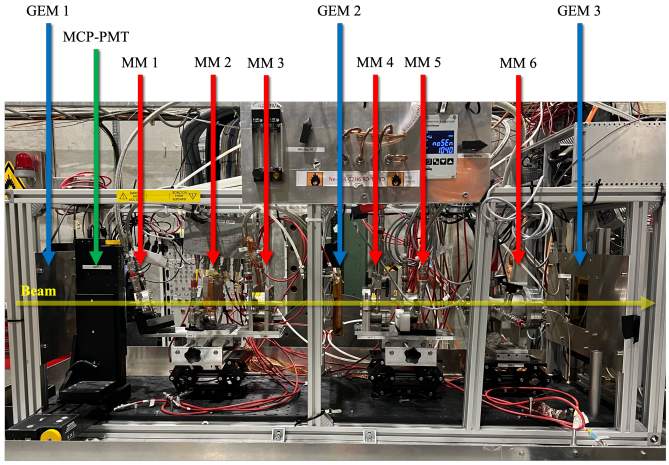

Figure 4: The beam telescope equipped with three triple-GEMs for particle tracking, an MCP-PMT for timing reference as well as DAQ trigger, and PICOSEC prototypes for testing.

Quantifying the time resolution of the PICOSEC detector requires a reference device with significantly superior timing precision. To fulfill this condition, the MCP-PMT with a time resolution below 6 ps in the central region [1, 2] serves as the reference for the PICOSEC prototypes. The devices are aligned to each other, ensuring that particles passed through the active area of both. To amplify and read out the signal, a custom-developed RF pulse amplifier cards optimized for PICOSEC (with built-in discharge protection up to 350 V, 650 MHz bandwidth, 38 dB gain, 75 mW power consumption [10, 17]) are used in conjunction with an oscilloscope.

In the analysis, the constant fraction discrimination (CFD) method is employed to determine the timestamp at which the signal reaches a specific fraction of its peak amplitude, thereby addressing the issue of time walk [1]. The leading edge of the electron peak is fitted with a sigmoid function to identify the signal position in time at 20% of the its amplitude. The SAT is calculated as the difference between the timestamps of the PICOSEC detector and the reference device. The SAT distribution is analysed using a double Gaussian fit and time resolution of the detector system is computed as the standard deviation of this distribution.

The results presented in this paper are derived from calculations conducted after applying several selection criteria (cuts) to the triggered events. Initially, a time window cut is implemented, selecting events within 300 ps of the median time difference of all recorded signals to exclude off-time events and noise fluctuations. Additional cuts are applied to set signal amplitude limits. Events with amplitudes below 1% of the dynamic range, categorised as empty events, and those above 99%, classified as saturated waveforms, are rejected. Furthermore, a geometrical cut is essential due to the Cherenkov radiator's emission of a UV photon cone at approximately 45-degree angle. To ensure accurate time resolution measurements, only fully contained events within the detector's active area should be included. Specifically, a cut of a 4 mm diameter circle around the pad center for a 10 mm diameter detector equipped with a 3 mm thick radiator (or a larger diameter, if otherwise specified) was implemented. Signals from tracks that pass outside this central region show reduced amplitude because of the partial loss of N_{PE} beyond the area of the channel.

4. Photocathode characterisation

Three different photocathode materials including Cesium Iodide, Diamond-Like Carbon and Boron Carbide have been examined. The fabrication, characterisation and performance evaluation of these photocathode materials have been detailed, highlighting their strengths and challenges in achieving precise timing in advanced detection systems. To ensure consistency of the results, all measurements presented in this paper were performed using identical single-pad non-resistive detectors featuring a 10 mm diameter active area (or 15 mm if otherwise specified), with pre-amplification and amplification gaps of approximately 127 µm. The detectors were operated in a sealed mode, maintaining a gas pressure of 990 ± 5 mbar for the purpose of comparison.

4.1. Cesium Iodide

Cesium Iodide is the most widely used material for photocathodes in gaseous radiation detectors due to its high QE and its sensitivity to UV radiation. The baseline photocathode used in the PICOSEC detector consists of an 18 nm thick CsI layer deposited onto a 3 mm thick MgF_2 substrate with a 3 nm thick Cr conductive interfacial layer, exceeding 12 photoelectrons per MIP [1], Previous studies on transparency in the VUV range have shown that the pure MgF_2 substrate has approximately 80% transparency, which decreases to 45% with the addition of the Cr layer, and further to 10% with the CsI layer [5].

Particle beam measurements were performed using a PICOSEC prototype equipped with a CsI photocathode, operated in a sealed mode at a gas pressure of 985 mbar. At voltage settings of V_C = -430 V on the cathode and V_A = 265 V on the anode, the detector exhibited a time resolution of σ = 15.8 ± 2.2 ps, as illustrated in Fig. 5.

Despite exhibiting excellent time resolution, CsI is vulnerable to damage from ion backflow, discharges and humidity. Fig. 6 illustrates the decline in QE observed in a CsI sample before and after multiple irradiation steps, providing evidence of ion bombardment affecting CsI. Studies demonstrated that after accumulating a charge of 6 mC/cm^2, the QE for CsI decreased by 80%, whereas for B_4C, it decreased by 45%, indicating a more rapid degradation of CsI [5]. One possible solution to reduce the impact of ion backflow on CsI and mitigate degradation involves introducing protective layers, such as MgF_2 or Lithium Fluoride (LiF) [18]. Nonetheless, tests conducted within the PICOSEC project revealed that these layers inhibited electron extraction, leading to reduced QE [5]. Another approach to address the issue of non-robustness is to explore alternative materials, with carbon-based photocathodes like DLC and B_4C being the most promising candidates.

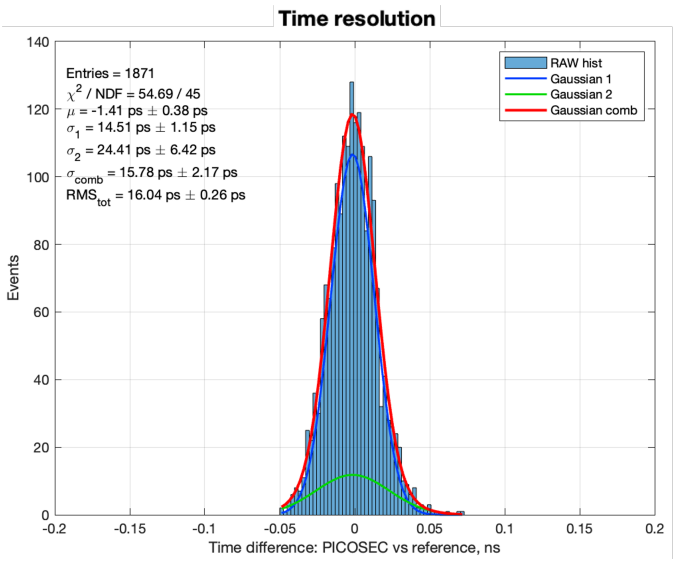

Figure 5: SAT distribution of a single-pad prototype, featuring a 10 mm diameter active area, equipped with an 18 nm thick CsI photocathode with a 3 nm thick Cr conductive layer, operated in a sealed mode at a gas pressure of 985 mbar. The voltage settings were V_C = -430 V on the cathode and V_A = 265 V on the anode. The histogram consists of the data after implementing a geometrical cut of a 4 mm diameter circle around the pad center to include only fully contained events. The results of a double Gaussian fit yield a time resolution of σ = 15.8 ± 2.2 ps.

4.2. *Diamond-Like Carbon*

Diamond-Like Carbon represents an alternative photocathode material that offers greater resistance to environmental influences compared to CsI. DLC belongs to a class of amorphous carbon materials, exhibiting excellent properties including chemical and thermal stability, hardness and robustness. Initial measurements of DLC photocathodes have been conducted by collaborators from USTC [13], including tests of various layer thicknesses, measurements of QE, NPE and time resolution as well as aging studies. DLC samples consistently demonstrated good performance and robustness, making them a strong candidate for PICOSEC photocathodes.

The DLC photocathodes presented in this paper were fabricated using a magnetron sputtering technique at the CERN Micro-Pattern Technologies (MPT) workshop. DLC photocathodes with thicknesses ranging from 1 nm to 100 nm were deposited on glass and MgF_2 substrates, with some samples including a Cr interfacial layer. Fig. 7 depicts the DLC photocathodes with the various thicknesses produced during one of the two deposition campaigns. The process proved to be reproducible across both campaigns.

Profilometer measurements were performed to investigate the thicknesses of the 50 nm and 100 nm layers. For layers in the range of a few nanometers, specifically from 1.5 nm to 4.5 nm, thicknesses were estimated by scaling the coating time. Fig. 8 presents the results of transparency measurements conducted in the wavelength range from 200 nm to 800 nm using a spectrophotometer. The data demonstrate a correlation between the estimated thicknesses and the measured transparency.

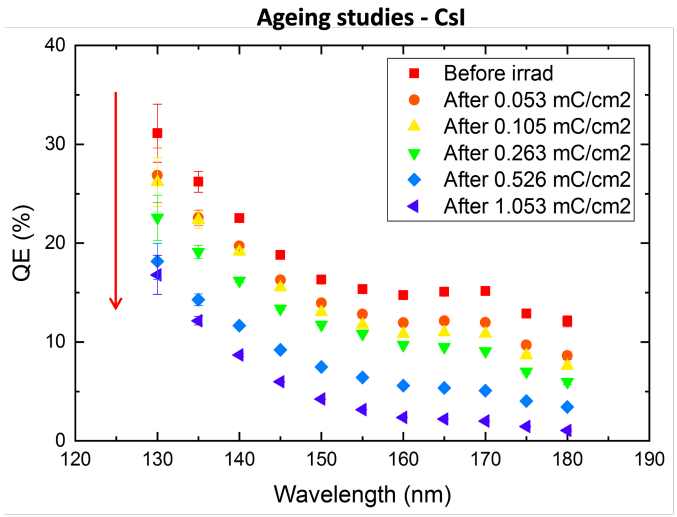

Figure 6: Ageing studies of a CsI photocathode performed in the ASSET setup: Decrease in QE after multiple irradiation steps, indicating the impact of ion bombardment on CsI [5].

The transparency of samples with a thickness of a few nanometers in the VUV range is approximately 60%.

Surface resistivity measurements were conducted, exhibiting a correlation between the thickness of the DLC layer and its resistivity, as shown in Fig. 9. The higher resistivity of the DLC photocathodes on the MgF_2 radiator compared to the glass substrate suggests that the layer deposited on the MgF_2 is thinner, potentially due to the lower adhesion of the crystal.

The DLC photocathodes, with thicknesses ranging from 1.5 nm to 3.5 nm, were characterised during particle beam measurements. The measurements were performed at a gas pressure of 990 mbar. The NPE generated by the DLC photocathodes varied between 2.5 and 3. The 10 mm diameter active area detector featuring a 1.5 nm thick DLC photocathode deposited directly on the radiator and operated at voltages of V_C = -500 V on the cathode and V_A = 275 V on the anode demonstrated the best performance, achieving a time resolution of σ = 31.9 ± 1.3 ps, as illustrated in Fig. 10. Thicker samples

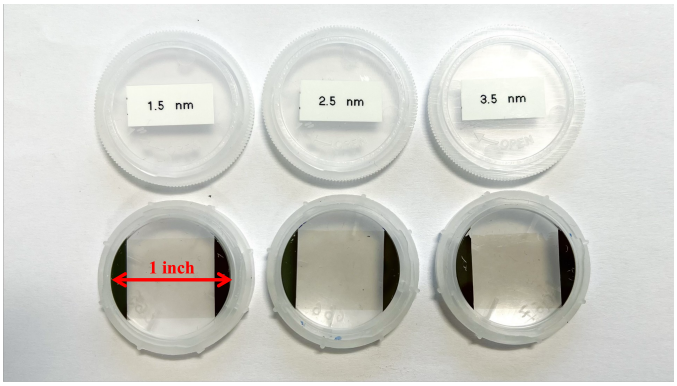

Figure 7: Picture of DLC photocathodes with various layer thicknesses deposited at the CERN MPT workshop using a magnetron sputtering technique.

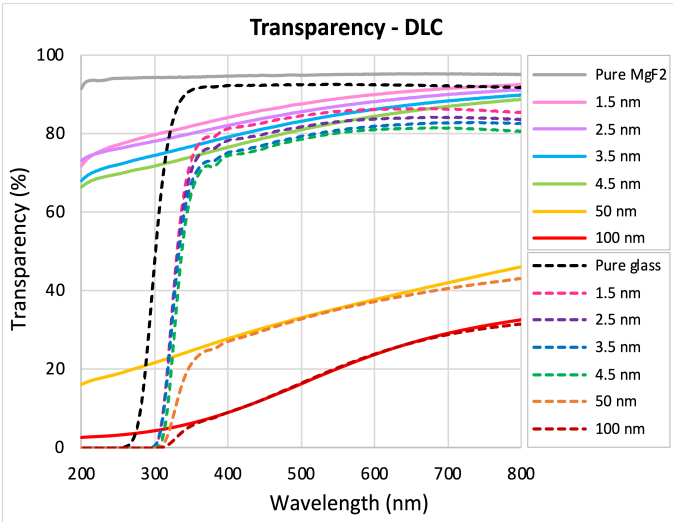

Figure 8: Transparency measurements of the DLC layers with thicknesses ranging from 1.5 nm to 100 nm deposited on MgF_2 and glass substrates, conducted in the wavelength range from 200 nm to 800 nm using a spectrophotometer.

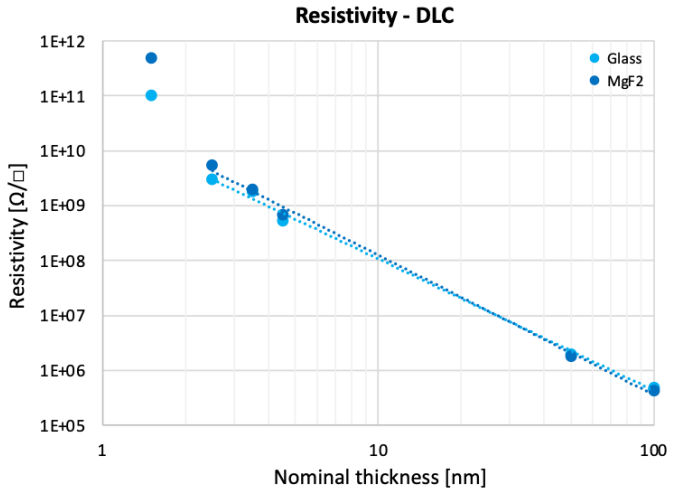

Figure 9: Surface resistivity measurements of the DLC photocathodes, presenting a correlation between estimated thicknesses and resistivity. The higher resistivity of the DLC photocathodes on the MgF_2 radiator compared to the glass substrate suggests a thinner deposited layer on the MgF_2, possibly due to lower crystal adhesion.

exhibited comparable time resolution values, with a deviation of approximately 4 ps.

The DLC photocathodes deposited directly on the radiator without a Cr conductive interfacial layer are sufficient for studying photocathode performance. Nonetheless, in high-rate environments, a Cr layer is essential to mitigate charging-up effects and voltage drops, particularly for samples with larger surface areas. Consequently, samples with Cr were evaluated, showing a decrease in transparency of approximately 30% and 2 ps worse time resolution.

To enhance UV photon production, a thicker radiator was introduced. At the same time, the Cherenkov cone diameter was widened. A prototype with a 15 mm diameter active area, equipped with a 2.5 nm thick DLC photocathode deposited on a 5 mm thick MgF_2 radiator, was tested. The analysis involved applying a geometric cut, consisting of a 5 mm diameter circle around the pad center, to include only fully contained events. The detector operated at of V_C = -490 V on the cathode and V_A = 275 V on the anode yielded a time resolution of $\sigma = 28.0 \pm 1.4$ ps.

4.3. Boron Carbide

Boron Carbide is a chemical compound from the carbide group, known for its crystalline structure and exceptional hardness, often used as a substitute for diamond. The initial B_4C photocathodes were developed at CEA, where a wide range of thicknesses was tested, yielding promising results [2, 11]. More detailed studies discussed in this paper were conducted with B_4C samples fabricated using a sputtering technique at ESS. During the coating campaigns, B_4C photocathodes with thicknesses ranging from 7 nm to 15 nm were deposited on MgF_2 radiators with a Cr conductive interfacial layers.

Profilometer measurements were conducted to determine the thickness of the photocathodes. The 7 nm layer was estimated based on the scaling of the coating time, considering the machine's resolution limits. Transparency measurements of the B_4C layers, conducted in the VUV wavelength range, demonstrated a correlation between estimated thicknesses and transparency, with values ranging from 40% for the thinnest layer to 20% for the thickest.

The B_4C photocathodes were evaluated through particle beam measurements. The prototypes were operated at a gas pressure of 990 mbar. The NPE created by the B_4C photocathodes ranged between 2 and 4, with higher PE production observed in thinner layers. The detector equipped with a 9 nm thick B_4C photocathode and operated at V_C = -490 V on the cathode and V_A = 275 V on the anode, exhibited the best performance, achieving a time resolution of $\sigma = 34.5 \pm 1.5$ ps, as shown in Fig. 11. The time resolution of the remaining B_4C samples decrease, with the thickest sample showing a degradation of approximately 10 ps.

5. Discussion

In the comparative analysis of photocathode materials, distinct performance characteristics were observed among CsI, DLC, and B_4C. CsI exhibited the highest QE, exceeding 12 photoelectrons per MIP, whereas DLC yielded QE values ranging between 2.5 and 3, while B_4C between 2 and 4. Despite B_4C being more transparent than DLC, both materials exhibit similar efficiency, generating comparable NPE. NPE correlates with the achievable time resolution. CsI showcased the best performance with $\sigma \approx 15.8$ ps, followed by DLC with $\sigma \approx 32$ ps and B_4C with $\sigma \approx 34.5$ ps. Although demonstrating excellent timing results, CsI also exhibited a faster degradation in QE compared to carbon-based materials. Furthermore, carbon-based materials displayed notably greater resistance to humidity. Considering the demand for robust detectors with

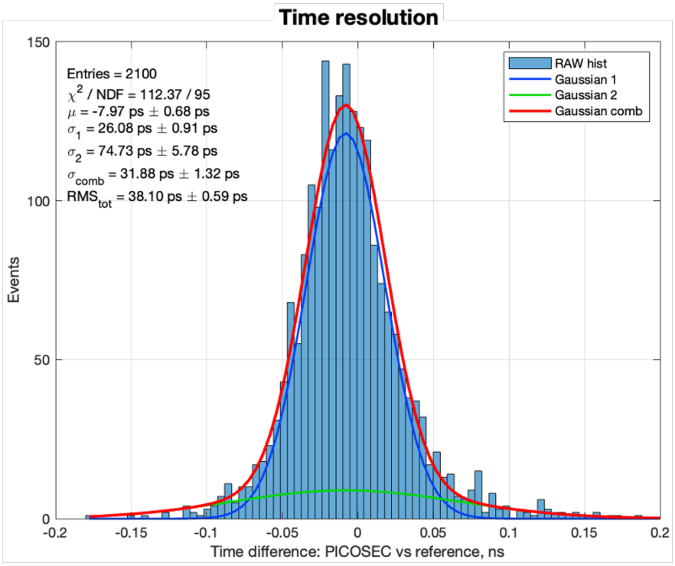

Figure 10: SAT distribution of a prototype equipped with a 1.5 nm DLC photocathode. The voltage settings were V_C = -500 V on the cathode and V_A = 275 V on the anode. The results show a time resolution of σ = 31.9 ± 1.3 ps.

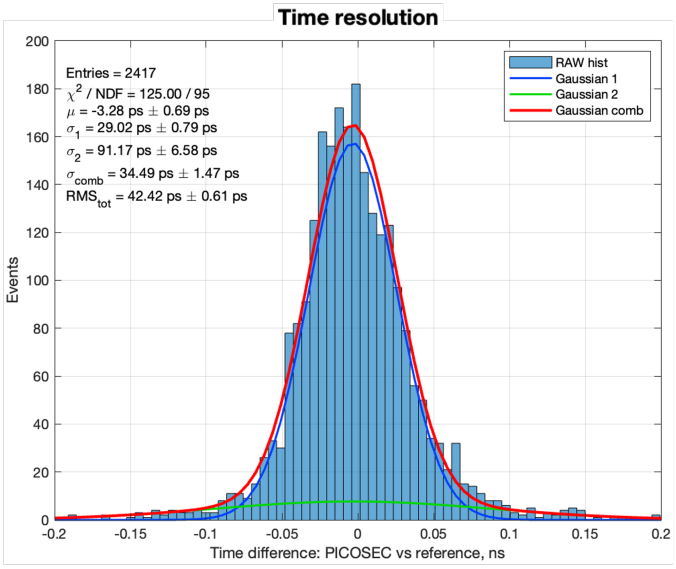

Figure 11: SAT distribution of a prototype equipped with a 9 nm B_4C photocathode. The voltages were at V_C = -490 V on the cathode and V_A = 275 V on the anode. The results show a time resolution of σ = 34.5 ± 1.5 ps.

timing specifications that allow a margin on operating condition, DLC and B_4C emerge as promising candidates. Consequently, a detector configuration comprising a single-pad prototype with a 15 mm diameter active area resistive Micromegas of 20 MΩ/□, utilising a 1.5 nm DLC photocathode and an amplifier integrated on the outer PCB, was tested. Operating the device at V_C = -530 V on the cathode and V_A = 275 V on the anode, a time resolution of σ = 31.4 ± 0.6 ps was achieved within a 9 mm diameter circle around the pad center, including only fully contained events. A uniform time response across this region, with an RMS = 38.8 ± 0.3 ps, was observed, as depicted in Fig. 12.

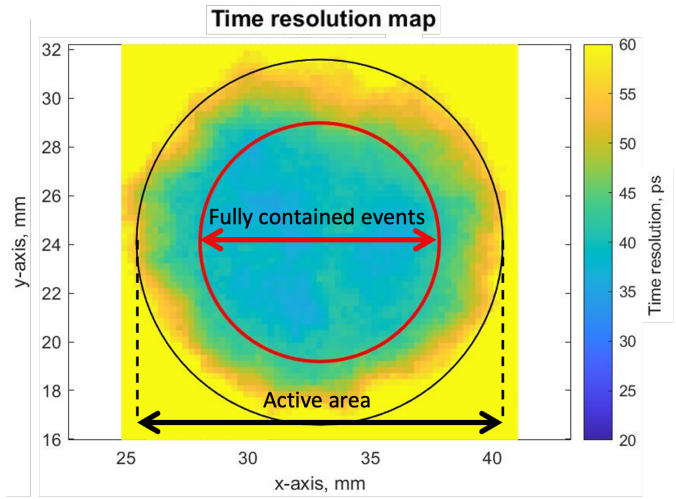

Figure 12: Time resolution map of a detector configuration consisting of a 15 mm diameter active area resistive Micromegas of 20 MΩ/□, a 1.5 nm DLC photocathode and an integrated amplifier. The black circle indicates the active area of the detector, while the red circle highlights fully contained events.

6. Conclusions

The work described in this paper is focused on enhancing the robustness of PICOSEC detectors. The research delves into the characterisation of robust carbon-based photocathodes, such as DLC and B_4C. Results obtained from prototypes equipped with DLC and B_4C photocathodes revealed time resolutions of approximately $\sigma \approx 32$ ps and $\sigma \approx 34.5$ ps, correspondingly. Efforts dedicated to detector developments increase the feasibility of the PICOSEC concept for experiments requiring sustained performance while maintaining excellent timing precision. Current developments include research on alternative materials, such as titanium to replace Cr, and carbon-based nanostructures for use as photocathodes. Simultaneously, a 10×10 cm^2 robust photocathode, incorporating a conductive interlayer to prevent a voltage drop, will be tested with a 100-channel prototype [10] and a SAMPIC digitiser [19]. In view of improving the stability of the detector, the production of a high-rate 10×10 cm^2 Micromegas with double-layer DLC for vertical charge evacuation and evaluation of rate capability is ongoing. Additionally, efforts to enhance spatial resolution involve testing high-granularity layouts. Scaling up the PICOSEC detector by tiling 10×10 cm^2 modules or developing larger prototypes are the next steps.

Acknowledgements

We acknowledge the support of the CERN EP R&D Strategic Programme on Technologies for Future Experiments; the RD51 Collaboration, in the framework of RD51 common projects; the DRD1 Collaboration; the PHENIICS Doctoral School Program of Université Paris-Saclay, France; the Cross-Disciplinary Program on Instrumentation and Detection of CEA, the French

Alternative Energies and Atomic Energy Commission; the French National Research Agency (ANR), project id ANR-21-CE31-0027; the Program of National Natural Science Foundation of China, grants number 11935014 and 12125505; the COFUND-FP-CERN-2014 program, grant number 665779; the Fundação para a Ciência e a Tecnologia (FCT), Portugal; the Enhanced Eurotalents program, PCOFUND-GA-2013-600382; the US CMS program under DOE contract No. DE-AC02-07CH11359; this material is based upon work supported by the U.S. Department of Energy, Office of Science, Office of Nuclear Physics under contracts DE-AC05-06OR23177.

References

[1] J. Bortfeldt, et al., for the PICOSEC Micromegas Collaboration, *PICOSEC: Charged particle timing at sub-25 picosecond precision with a Micromegas based detector*, Nuclear Instruments and Methods in Physics Research A **903** (2018) 317–325.

[2] L. Sohl, *Development of PICOSEC-Micromegas for fast timing in high rate environments*, PhD dissertation, Université Paris-Saclay, 2020; available at https://hal-universite-paris-saclay.archives-ouvertes.fr/tel-03167728/.

[3] J. Bortfeldt, et al., for the PICOSEC Micromegas Collaboration, *Modeling the timing characteristics of the PICOSEC Micromegas detector*, Nuclear Instruments and Methods in Physics Research A **993** (2021) 165049.

[4] S. Aune, et al., for the PICOSEC Micromegas Collaboration, *Timing performance of a multi-pad PICOSEC-Micromegas detector prototype*, Nuclear Instruments and Methods in Physics Research A **993** (2021) 165076.

[5] M. Lisowska, *Photocathode characterisation and ageing studies for precise-timing gaseous detectors*, MSc thesis, Wroclaw University of Science and Technology, 2021; available at https://cds.cern.ch/record/2885929?ln=en.

[6] A. Kallitsopoulou, *Development of a Simulation Model and Precise Timing Techniques for PICOSEC-Micromegas Detectors*, MSc thesis, Aristotle University of Thessaloniki, 2021; available at arXiv:2112.14113.

[7] I. Maniatis, *Research and Development of Micromegas Detectors for New Physics Searches*, PhD dissertation, Aristotle University of Thessaloniki, 2022; available at: http://ikee.lib.auth.gr/record/339482/files/GRI-2022-35238.pdf.

[8] E. Chatzianagnostou, *Study of multi-pad PICOSEC-MicroMegas detector prototype: Time resolution evaluation*, MSc thesis, Aristotle University of Thessaloniki, 2022; available at: http://ikee.lib.auth.gr/record/343732/files/GRI-2022-37581.pdf.

[9] M. Lisowska, et al., for the PICOSEC Micromegas Collaboration, *Sub-25 ps timing measurements with 10×10 cm^2 PICOSEC Micromegas detectors*, Nuclear Instruments and Methods in Physics Research A **1046** (2023) 167687.

[10] A. Utrobicic, et al., for the PICOSEC Micromegas Collaboration, *A large area 100-channel PICOSEC Micromegas detector with time resolution at the 20 ps level*, Journal of Instrumentation **18** (2023) C07012.

[11] M. Lisowska, et al., for the PICOSEC Micromegas Collaboration, *Towards robust PICOSEC Micromegas precise timing detectors*, Journal of Instrumentation **18** (2023) C07018.

[12] A. Utrobicic, et al., for the PICOSEC Micromegas Collaboration, *Single channel PICOSEC Micromegas detector with improved time resolution*, 2024; available at arXiv:2406.05657.

[13] X. Wang, et al., for the PICOSEC Micromegas Collaboration, *A Novel Diamond-like Carbon based photocathode for PICOSEC Micromegas detector*, 2024; available at arXiv:2406.08712.

[14] The CMS and TOTEM Collaborations *ALICE Technical Design Report of the High Momentum Particle Identification Detector*, CERN-LHCC-98–19, ALICE-TDR-1, 1998; available at: https://alice-collaboration.web.cern.ch/sites/default/files/Documents/PROJECTS/HMPID/HMPID_TDR.pdf

[15] H. Hödlmoser, *Development of Large Area CsI Photocathodes for the ALICE/HMPID RICH Detector*, PhD dissertation, Technischen Universität Wien, 2005; available at https://cds.cern.ch/record/924378/

[16] S. Martoiu, et al., *Development of the scalable readout system for micro-pattern gas detectors and other applications*, Journal of Instrumentation **18** (2013) C03015.

[17] C. Hoarau, et al., *RF pulse amplifier for CVD-diamond particle detectors*, Journal of Instrumentation **16** (2021) T04005.

[18] A Buzulutskov, a Breskin, R Chechik, J Va'vra, *Study of photocathode protection with thin dielectric films*, Nuclear Instruments and Methods in Physics Research A **371** (1996) 147-150.

[19] D. Breton, et al., *Measurements of timing resolution of ultra-fast silicon detectors with the SAMPIC waveform digitizer*, Nuclear Instruments and Methods in Physics Research A **835** (2016) 51-60.